Available online at www.sciencedirect.com

ScienceDirect

Geochimica et Cosmochimica Acta 238 (2018) 1–15

Geochimica et Cosmochimica Acta

www.elsevier.com/locate/gca

Iron isotope fractionation during magmatic-hydrothermal evolution: A case study from the Duolong porphyry Cu-Au deposit, Tibet

Jin-Xiang Li [a,b,*], Ke-Zhang Qin [b,c], Guang-Ming Li [b,c], Noreen J. Evans [d], Fang Huang [e], Jun-Xing Zhao [c]

[a] *Key Laboratory of Continental Collision and Plateau Uplift, Institute of Tibetan Plateau Research, Chinese Academy of Sciences, Beijing 100101, China*

[b] *CAS Center for Excellence in Tibetan Plateau Earth Sciences, Beijing 100101, China*

[c] *Key Laboratory of Mineral Resources, Institute of Geology and Geophysics, Chinese Academy of Sciences, Beijing 100029, China*

[d] *John de Laeter Center, TIGeR, Applied Geology, Curtin University, Perth, WA 6945, Australia*

[e] *CAS Key Laboratory of Crust-Mantle Materials and Environments, School of Earth and Space Sciences, University of Science and Technology of China, Heifei 230026, China*

Received 13 October 2017; accepted in revised form 3 July 2018; Available online 11 July 2018

Abstract

Ore-forming fluids ultimately precipitate Fe-bearing sulfides and oxides in hydrothermal ore deposits and the Fe isotopic composition of these minerals can trace magmatic-hydrothermal evolution. Here, we report on the Fe isotopic compositions of a suite of hydrothermal minerals (magnetite, pyrite, and chalcopyrite) and granodiorite porphyry from the giant Duolong porphyry Cu-Au deposit (Bolong and Duobuza section), central Tibet. Most magnetite grains with potassic alteration show only minor δ^{57}Fe variation (0.38 ± 0.07‰ to 0.52 ± 0.04‰ in Bolong and 0.68 ± 0.02‰ to 0.77 ± 0.08‰ in Duobuza), consistent with the equilibrium fluid δ^{57}Fe (~−0.3‰ and ~−0.1‰, respectively) at ~550–480 °C. The equilibrium fluids have lighter Fe isotope signatures than the Duolong granodiorite porphyry (δ^{57}Fe = 0.03 ± 0.06‰ to 0.07 ± 0.02‰), corroborating the hypothesis that exsolved fluids should have a lighter Fe isotopic composition relative to parental magmas. Chalcopyrite from the mineralized Bolong and Duobuza porphyries have relatively consistent δ^{57}Fe values of -0.60 ± 0.07‰ to -0.42 ± 0.07‰ and -0.40 ± 0.08‰ to -0.30 ± 0.05‰, respectively, with equilibrium fluids at ~450–350 °C having lighter δ^{57}Fe values of ~−0.7‰ and ~−0.6‰. The trend of decreasing δ^{57}Fe values in evolved fluids likely reflects Rayleigh fractionation of magnetite enriched in heavy Fe isotopes. This supposition is supported by the lighter δ^{57}Fe value (0.25 ± 0.07‰) recorded in magnetite that equilibrated with a lighter δ^{57}Fe fluid (~−0.5‰) at ~470 °C. Compared to chalcopyrite, pyrite from the Bolong and Duobuza sections have heavier δ^{57}Fe values of 0.35 ± 0.06‰ to 0.71 ± 0.06‰ and 0.53 ± 0.06‰ to 0.71 ± 0.07‰, respectively. The pyrite values correlate variably with the Fe isotopic composition of ore-forming fluids (δ^{57}Fe = −0.6‰ to −0.7‰), likely due to variations in the degree of Fe isotope exchange between pyrite and fluid. Moreover,

* Corresponding author at: Key Laboratory of Continental Collision and Plateau Uplift, Institute of Tibetan Plateau Research, Chinese Academy of Sciences, Beijing 100101, China. Fax: +86 10 84097079.

E-mail address: ljx@itpcas.ac.cn (J.-X. Li).

https://doi.org/10.1016/j.gca.2018.07.008

combined with previously published Fe isotopic compositions of hydrothermal minerals from oxidized and reduced ore deposits, the results show that chalcopyrite in oxidized hydrothermal deposits always has a lighter Fe isotopic composition than chalcopyrite from reduced hydrothermal deposits. This is likely controlled by melt composition and precipitation of magnetite/pyrrhotite-bearing mineral assemblages. Therefore, the Fe isotopic composition of chalcopyrite could be a useful diagnostic tool for distinguishing oxidized from reduced fluids in hydrothermal systems.

Keywords: Fe isotope; Magmatic-hydrothermal evolution; Porphyry Cu-Au deposit; Duolong; Tibet

1. INTRODUCTION

It is well known that metal-rich fluids exsolved from oxidized and reduced magmas play a key role in the formation of various types of hydrothermal ore deposits, including porphyry Cu ± Mo ± Au, skarn Cu ± Fe ± Zn, and skarn/vein Sn-W deposits (e.g., Audétat et al., 2000; Einaudi et al., 2003; Cooke et al., 2005; Sillitoe, 2010; Richards, 2011; Fontboté et al., 2017). Traditionally, oxygen, sulfur, and hydrogen isotopic signatures of hydrothermal minerals have been extensively used to reveal the source and evolution of ore-forming fluids (e.g., Rye, 1993; Hedenquist et al., 1998; Li et al., 2016a). In recent years, experimental studies have determined non-traditional iron (Fe) isotope fractionation factors between minerals (e.g., magnetite, pyrite, and chalcopyrite), fluid, and melt (e.g., Heimann et al., 2008; Polyakov and Soultanov, 2011; Syverson et al., 2013, 2017; Dauphas et al., 2017), and this important development means Fe isotopes can be added to the analytical toolbox for investigating magmatic-hydrothermal evolution and metal sources (e.g., Graham et al., 2004; Markl et al., 2006; Li et al., 2010, 2016a; Wang et al., 2011; Wawryk and Foden, 2015, 2017; Günther et al., 2017). Previous studies mainly focused on iron oxide-apatite deposits (Bilenker et al., 2016), skarn Fe-Cu-Au deposits (Wang et al., 2011, 2015, 2017; Zhu et al., 2016), skarn/vein Sn-W deposits (Wawryk and Foden, 2015), and carbonated-hosted Pb-Zn deposits (Gagnevin et al., 2012). However, systematic Fe isotope studies for porphyry Cu-Au deposits are scare.

Generally, the fluids exsolved from magmas have light Fe isotopic compositions because the Fe^{2+} species in fluids preferentially incorporates the light isotope (Simon et al., 2004; Heimann et al., 2008; Hill et al., 2010; Saunier et al., 2011; Wang et al., 2011, 2015; Telus et al., 2012). However, the variation of Fe isotopic compositions in evolved fluids are likely controlled by the different mineral assemblages precipitating in oxidized porphyry Cu-Au and reduced Sn-W hydrothermal systems (Wawryk and Foden, 2015, 2017). It is still unclear whether Fe isotope could be as a good tracer to evolution of ore-forming fluid. The Duolong deposit is a porphyry Cu-Au deposit in a continent arc setting (Tibet; Li et al., 2013, 2018) and provides an opportunity to study Fe isotope variations in porphyry-related hydrothermal system. In this study, the Fe isotopic values of granodiorite porphyry and hydrothermal minerals (magnetite, pyrite, and chalcopyrite) from the Duolong porphyry Cu-Au deposit (Tibet; Li et al., 2013) are presented in order to evaluate magmatic-hydrothermal evolution and the key factors controlling Fe isotope variation. Moreover, combined with previously published Fe isotopic data from other deposits (e.g., Wang et al., 2011, 2015; Wawryk and Foden, 2015; Li et al., 2016a), we discuss whether mineral Fe isotopic composition is a potentially useful tool for distinguishing different types of hydrothermal ore deposits.

2. GEOLOGICAL SETTING

The Tibetan plateau consists of five terranes (from north to south: Qaidam, Songpan–Ganze, Qiangtang, Lhasa, and India), separated by four Mesozoic and Cenozoic sutures (Ayimaquin–Kunlun, Jinshajiang, Bangong–Nujiang, and Indus–Yarlung, respectively; Fig. 1a and b; Yin and Harrison, 2000; Kapp et al., 2005; Zhang et al., 2012; Zhu et al., 2013). The Qiangtang terrane is divided by the Mesozoic Longmu-Shuanghu suture (LSS) into the northern and southern Qiangtang terrane (Fig. 1b; Zhai et al., 2011; Zhang et al., 2012; Zhu et al., 2013). During

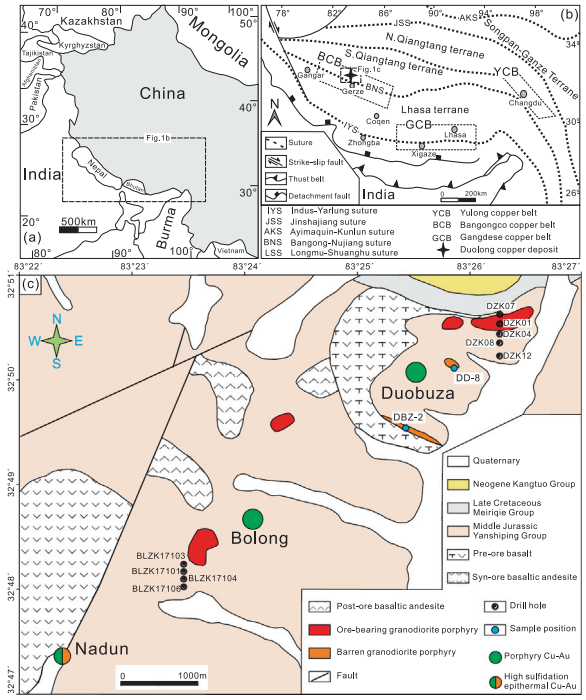

Fig. 1. (a) Geographic map, (b) sketch tectonic map (Hou et al., 2004) and generalized geologic map (c) of the Duolong porphyry Cu-Au deposit (Li et al., 2013).

northward subduction of the Bangong-Nujiang oceanic lithosphere, Jurassic-Cretaceous arc magmatism, including intermediate–felsic intrusions and volcanic rocks, was extensive in the southern Qiangtang terrane (Guynn et al., 2006; Zhang et al., 2012; Li et al., 2014a, 2014b, 2016c; Liu et al., 2014, 2017; Huang et al., 2015; Geng et al., 2016; Hao et al., 2016; Wu et al., 2016; Zhu et al., 2016). The giant Duolong porphyry–high sulfidation epithermal Cu–Au district is located approximately 100 km northwest of Gerze city (Fig. 1b) and is closely related to Early Cretaceous arc magmatism (~118 Ma; Li et al., 2013, 2016a, 2016b, 2017; Zhu et al., 2015; Hou and Zhang, 2015; Sun et al., 2017). The Cu–Au district (prospective metal resources of ~25 Mt Cu and ~400 t Au) covers more than 120 km^2, and includes the Duolong and Naruo porphyry deposits (Li et al., 2013; Sun et al., 2017) and the Rongna (or Tiegelongnan; Li et al., 2015; Duan et al., 2016; Lin et al., 2017) and Nadun porphyry-high sulfidation epithermal deposits (Li et al., 2016a). The Duolong porphyry Cu-Au deposit (5.4 Mt at 0.72% Cu, 41 t at 0.23 g/t Au; Li et al., 2012a), the focus of this study, is located in the southwest of the Duolong Cu-Au district and is divided into the Duobuza and Bolong sections (Fig. 1c). The stratigraphy in the Duolong deposit mainly comprises the Middle Jurassic Quse Group, Late Cretaceous Meiriqie Group, and Neogene Kangtuo Group (Fig. 1c). The Middle Jurassic Quse Group is a clastic-interbedded volcanic sequence of littoral facies composed of arkosic sandstone and siltstone-interbeded siliceous rock. The Late Cretaceous Meiriqie Group contains basaltic andesite, dacite, volcanic-clastic rocks, andesite porphyry and andesite. The Neogene Kangtuo Group is composed of brown-red clay and sandy gravel (Fig. 1c).

2.1. Magmatic activity

The intrusive rocks in the Duolong deposit mainly comprise ore-bearing and barren granodiorite porphyries, which intruded into the Middle Jurassic Quse Group as stocks and dykes (Fig. 1c). Meanwhile, ore-bearing quartz diorite porphyry intruded into ore-bearing granodiorite porphyry (Fig. 2a). Precise zircon U–Pb dating (Li et al., 2011, 2013, 2017; Sun et al., 2017; Zhu et al., 2015) indicated that these intrusions were synchronously emplaced at ~118 Ma, consistent with the molybdenite Re-Os ages (~118 Ma; Zhu et al., 2015; Sun et al., 2017). This suggests there is a genetic relationship between the intrusions and the Cu-Au mineralization. Additionally, pre-ore Early Cretaceous volcanic basalt ($^{40}Ar/^{39}Ar$ plateau age of ~142 Ma; Li et al., 2013) has alkaline features with an enrichment of high field strength elements (HFSE: Nb and Ta) and large ion lithophile elements (LILE: Rb and Ba; Li et al., 2016b), consistent with OIB-type magmas. Cretaceous basalt, basaltic andesite and andesite from the Late Cretaceous Meiriqie Group are syn- and post-ore volcanic rocks with zircon U–Pb ages of ~105–118 Ma (Li et al., 2011, 2016b).

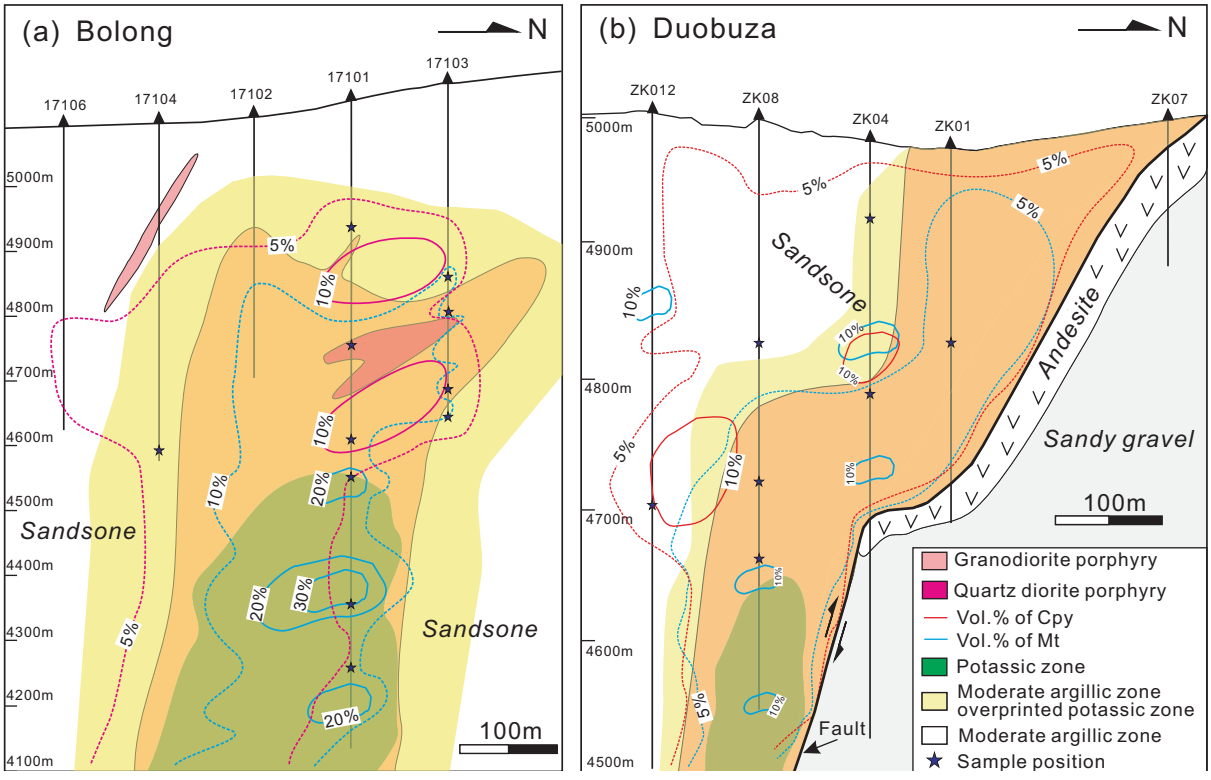

Fig. 2. Cross-section profiles of the Bolong (a) and Duobuza sections (b) in the Duolong porphyry Cu-Au deposit (Li et al., 2013). Spatial distribution of magnetite and chalcopyrite are shown by blue and red lines, respectively. The percentage values represent the volume fraction of magnetite and chalcopyrite. (For interpretation of the references to colour in this figure legend, the reader is referred to the web version of this article.)

Syn- and post-ore volcanic rocks, and ore-bearing/barren granodiorite porphyry show similar geochemical features with high-K calc-alkaline series classification, enrichment in large ion lithophile elements (LILE: such as Rb and Ba), and depletion of high field strength elements (HFSE: such as Nb and Ta), consistent with arc magmas (Li et al., 2013, 2016b).

2.2. Hydrothermal alteration

A wide range of hydrothermal alteration extends over an area of more than 10 km^2. The alteration zone can be divided into potassic, moderate argillic overprinted potassic, moderate argillic, and propylitic alteration from the ore-bearing porphyry center, outwards and upwards (Fig. 2a and b). Phyllic alteration is not well developed and quartz–sericite veinlets occur only locally (Li et al., 2012b), consistent with the typical alteration model for porphyry Cu-Au deposits (e.g., Liang et al., 2009; Sillitoe, 2010).

Potassic alteration zone: Secondary K-feldspar has primarily altered plagioclase phenocrysts but is also dispersed in the matrix and occurs as an alteration halo at the edge of quartz–chalcopyrite–magnetite veinlets (A-type, Fig. 3a and b; Gustafson and Hunt, 1975). Secondary biotite replaces hornblende and primary biotite while magnetite, quartz–K-feldspar ± magnetite, quartz–biotite–chalcopyrite, and biotite veinlets (EB-type, Gustafson and Quiroga, 1995) are also recognized in this alteration zone. Moreover, the potassic alteration zone is primarily developed at depth in the mineralized granodiorite porphyry and is superposed by moderate argillic alteration (i.e. *moderate argillic overprinted potassic alteration zone*; Fig. 2a and b). Hydrothermal magnetite developed primarily in the potassic alteration zone, in higher proportions in the Bolong section (~5–30 vol%) than in the Duobuza section (~5–10 vol%; Fig. 2a and b).

Moderate argillic zone: This zone extensively occurs in wall-rock sandstone and is superposed on the potassic alteration zone (Fig. 2a and b). It is characterized mainly by kaolinization and illitization–hydromuscovitation of plagioclase and chloritization of biotite (Li et al., 2012b). Quartz–chalcopyrite ± pyrite veinlets (with chalcopyrite ± pyrite in the center of the veinlet and an argillic alteration halo; B-type; Gustafson and Hunt, 1975), quartz–molybdenite–chalcopyrite–pyrite, chalcopyrite ± pyrite, and quartz–carbonate–sphalerite–galena–chalcopyrite–pyrite veinlets (Fig. 3f) also occur in this alteration zone.

Propylitic zone: This zone occurs mainly in pre-ore basalt at the Duobuza section. The alteration minerals are epidote, chlorite and carbonate. Chlorite replaces biotite phenocrysts along rims, cleavage and in cores, while the pseudomorphs of biotite are occasionally retained. Moreover, carbonate, quartz, epidote and other minerals fill in the amygdales in basaltic rocks (Li et al., 2012b).

2.3. Mineralization

The Duolong Cu-Au mineralization, dominantly occurring in the ore-bearing porphyry and at the wallrock contact zone, is associated with potassic and moderate argillic overprinted potassic alteration (Fig. 2a and b). Hypogene ore minerals are mainly chalcopyrite, followed by pyrite, and minor chalcocite, bornite and native gold. On the whole, there is more chalcopyrite than bornite and far more chalcopyrite than pyrite. Chalcopyrite occurs mainly as disseminated (Fig. 3e) and stockwork veinlets (Fig. 3a–c), while bornite occurs mainly as an exsolution phase in chalcopyrite (Li et al., 2012b). In general, hydrothermal magnetite is spatially related to with chalcopyrite (Fig. 2a and b), consistent with the mineralization characteristics of a typical porphyry Cu-Au deposit (e.g., Sillitoe, 2010; Sun et al., 2013). Petrographic observations suggest that magnetite may have formed slightly earlier than chalcopyrite (Fig. 3d). In addition, previous fluid inclusion and O-H-S isotope studies suggest that ore-forming fluids were exsolved from magmas and of primary magmatic origin for the Duolong alteration and mineralization (Li et al., 2007; Li, 2008). Hydrothermal magnetite in the potassic zone was formed at ~550–450 °C, whereas Cu-Au mineralization dominantly formed at ~450 to 350 °C (Li et al., 2007).

3. SAMPLING AND ANALYTICAL METHODS

3.1. Sampling and petrography

Two fresh granodiorite porphyries at the Duolong Cu-Au deposit (Fig. 1c) were sampled for Fe isotope analyses. They show porphyritic texture (30–40 vol% phenocrysts) and are composed of quartz (22–30 vol%), plagioclase (40–45 vol%), K-feldspar (10–15 vol%), amphibole (8–10 vol%), biotite (2–5 vol%) and accessory minerals (<1 vol%) including zircon, apatite, titanite, and Fe-Ti oxides.

Ten mineralized granodiorite porphyries, one quartz-diorite porphyry, and seven sandstones were collected from drill core (Fig. 2a and b) for separation of magnetite, pyrite, and chalcopyrite. Magnetite in selected porphyry samples occurs in disseminated and quartz–magnetite ± chalcopyrite veinlets (Fig. 3a and b). Massive magnetite in one porphyry sample BLZK17101-781 is associated with the potassic alteration and cut by quartz–pyrite–chalcopyrite veinlets (Fig. 3c). Pyrite and chalcopyrite from porphyries and sandstones mainly occur as disseminated grains (Fig. 3e) and in quartz ± magnetite–chalcopyrite–pyrite veinlets. However, Pyrite and chalcopyrite from two argillic sandstones in the Duobuza section (DZK04-79 and DZK012-300; Table 1) occur as disseminated grains and in quartz–chalcopyrite–pyrite–sphalerite–galena veinlets (Fig. 3f).

3.2. Analytical methods

Magnetite separates were obtained by magnetic separation from crushed samples. Pyrite and chalcopyrite were separated by hand-picking under a binocular microscope in Langfang Yuneng Company. Twenty-four sulfide (pyrite and chalcopyrite), nine magnetite separates, and two powders of fresh granodiorite porphyry whole rock were selected for Fe isotope analyses (Table 1). Dissolution and purification was carried out at the Institute of Geology

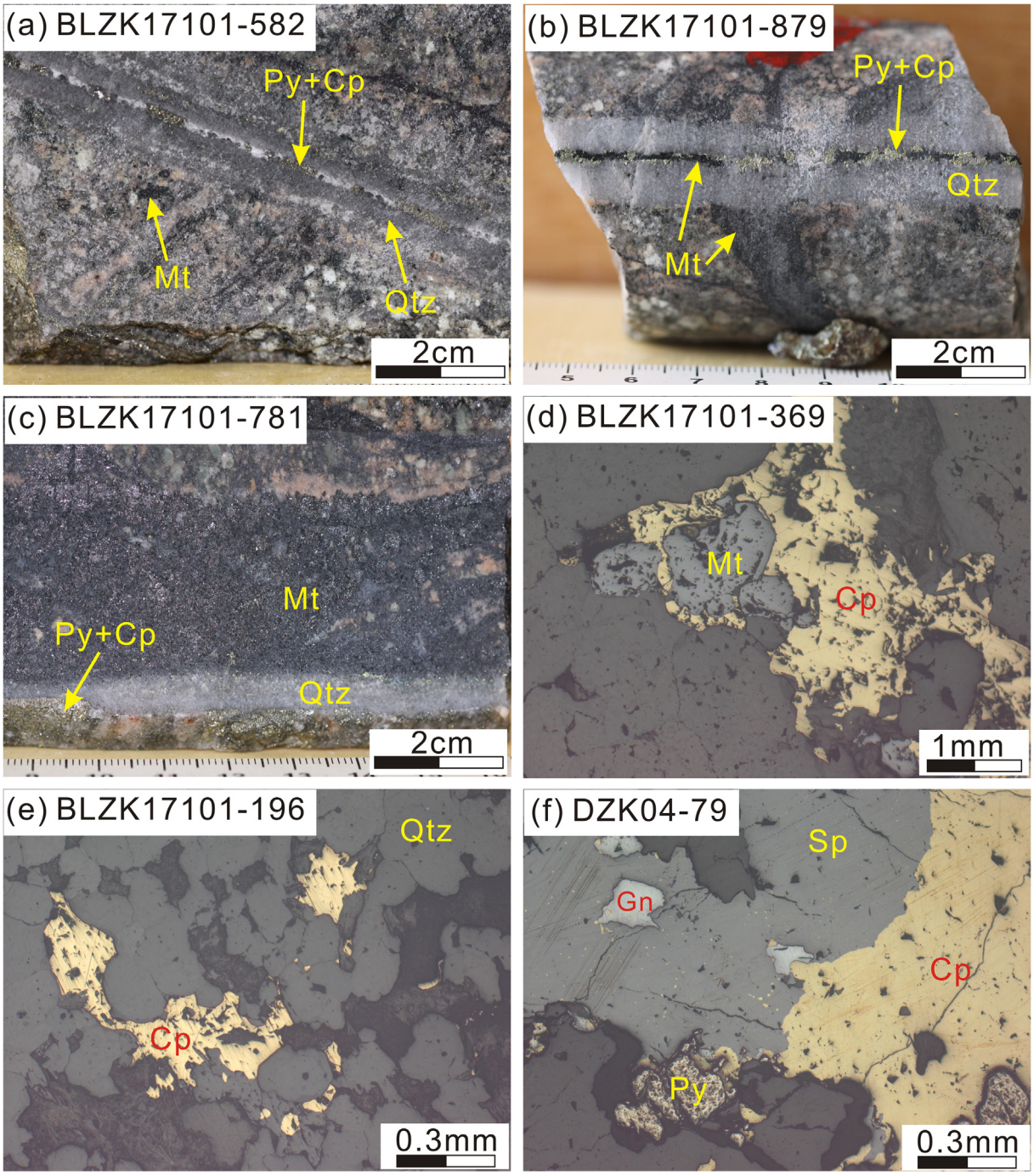

Fig. 3. Representative photographs showing occurrences of magnetite, chalcopyrite, and pyrite in the Duolong porphyry Cu-Au deposit. (a) Mt and biotite veinlets in potassic alteration zone cut by Qtz-Py-Cp veinlet (width ~ 1 cm). (b) Qtz-Mt-Cp veinlet cut by Qtz-Mt-Py-Cp veinlet (width ~ 1.5 cm) in potassic alteration zone. (c) Massive Mt with potassic alteration cut by Qtz-Py-Cp veinlets (width ~ 1 cm). (d) Mt surrounding by Cp in the moderate argillic overprinted potassic alteration zone. (e) Disseminated Cp in the moderate argillic zone. (f) Py-Cp-Sp-Gn mineral assemblage in Qtz-bearing veinlet (width ~ 1–2 cm) in the moderate argillic zone. Abbreviations: Mt, magnetite; Cp, chalcopyrite; Py, pyrite; Qtz, quartz; Sp, sphalerite; Gn, galena.

and Geophysics, Chinese Academy of Sciences (IGGCAS), following the established procedure (Zhao et al., 2015, 2017). Subsequently, the purified sample solutions were analyzed for Fe isotopes using a MC-ICP-MS (Thermo Neptune plus) at the University of Science and Technology of China (USTC), following previously published procedures (Huang et al., 2011; Gong et al., 2017; Xia et al., 2017; Zhao et al., 2017). Instrumental mass fractionation was corrected using standard-sample bracketing. Iron isotope data are reported in standard δ notation in per mil

Table 1
Fe isotopic compositions of sulfide, magnetite, and granodiorite porphyry from the Duolong Cu-Au deposit, central Tibet Abbreviations: Mt, magnetite; Cp, chalcopyrite; Py, pyrite; Qtz, quartz; Sp, sphalerite; Gn, galena; Cc, Carbonate; WR, whole rock.

Sample no.	Lithology and alteration	Description	Mineral	δ^{56}Fe (‰)	2SD	δ^{57}Fe (‰)	2SD	n
Bolong section								
BLZK17101-196	Argillic-sericitic sandstone	Disseminated Cp	Cp	−0.17	0.02	−0.25	0.03	3
BLZK17101-369	Potassic-argillic quartz diorite porphyry	Disseminated Mt, Qtz-Mt-Cp-Py vein	Cp	−0.36	0.03	−0.54	0.05	3
			Mt	0.28	0.02	0.42	0.04	3
BLZK17101-524	Argillic-potassic granodiorite porphyry	Disseminated Mt, Q-Mt-Cp and Qtz-Py-Cp veins	Cp	−0.31	0.02	−0.45	0.04	3
			Mt	0.27	0.03	0.40	0.05	3
BLZK17101-582	Argillic-potassic granodiorite porphyry	Disseminated Mt, Qtz-Py-Cp vein	Py	0.39	0.03	0.60	0.03	3
			Mt	0.26	0.05	0.40	0.07	3
BLZK17101-781	Potassic granodiorite porphyry	Disseminated Mt, Domiantly Qtz-Mt-Cp vein	Cp	−0.35	0.03	−0.52	0.04	3
			Mt	0.16	0.05	0.25	0.07	6
BLZK17101-879	Potassic granodiorite porphyry	Disseminated Mt, Qtz-Mt-Cp-Py vein	Cp	−0.41	0.04	−0.60	0.07	6
			Mt	0.25	0.03	0.38	0.07	3
BLZK17103-298	Argillic-hornfelsic sandstone	Disseminated Cp and Py, Qtz-Mt-Cp vein	Cp	−0.19	0.04	−0.28	0.02	3
			Py	0.48	0.04	0.71	0.06	6
BLZK17103-351	Argillic-sericitic granodiorite porphyry	Disseminated Cp and Py	Cp	−0.28	0.03	−0.42	0.07	6
			Py	0.23	0.03	0.35	0.06	3
BLZK17103-475	Argillic-potassic granodiorite porphyry	Disseminated Mt and Py, Qtz-Mt and Py-Cp vein	Py	0.39	0.04	0.58	0.06	6
			Mt	0.35	0.04	0.52	0.04	3
BLZK17103-508	Argillic-sericitic sandstone	Disseminated Cp, Qtz-Mt-Cp vein	Cp	−0.15	0.02	−0.22	0.02	3
BLZK17104-504	Argillic sandstone	Disseminated Cp, Qtz-Cc-Cp vein	Cp	−0.15	0.01	−0.23	0.07	3
Duobuza section								
DZK01-145	Argillic-potassic granodiorite porphyry	Disseminated Mt and Cp, Qtz-Mt-Cp vein	Cp	−0.20	0.03	−0.30	0.05	3
			Py	0.44	0.03	0.66	0.03	3
			Mt	0.47	0.03	0.70	0.07	3
DZK04-79	Argillic sandstone	Disseminated Cp, Qtz-Py-Cp-Sp-Gn vein	Cp	−0.33	0.04	−0.50	0.05	3
DZK04-198	Argillic-potassic granodiorite porphyry	Disseminated Cp, Qtz-Cp-Py vein	Cp	−0.27	0.04	−0.40	0.08	3
			Py	0.36	0.01	0.53	0.06	3
DZK08-172	Argillic sandstone	Disseminated Mt and Cp, Qtz-Mt-Cp vein	Cp	−0.25	0.04	−0.38	0.07	6
			Py	0.38	0.04	0.58	0.08	6
DZK08-270	Potassic-argillic granodiorite porphyry	Disseminated Mt and Cp, Qtz-Mt-Cp vein	Cp	−0.22	0.01	−0.33	0.03	3
			Mt	0.52	0.03	0.77	0.08	3
DZK08-338	Potassic-argillic granodiorite porphyry	Disseminated Mt and Cp, Qtz-Mt-Cp vein	Cp	−0.23	0.04	−0.35	0.06	4
			Mt	0.45	0.03	0.68	0.02	3
DZK012-300	Argillic sandstone	Disseminated Cp and Py, Qtz-Py-Cp-Sp vein	Cp	−0.32	0.04	−0.48	0.08	6
			Py	0.47	0.02	0.71	0.07	3
DD-8	Fresh granodiorite porphyry		WR	0.02	0.03	0.03	0.06	3
DBZ-2	Fresh granodiorite porphyry		WR	0.05	0.02	0.07	0.02	3
BHVO-2	Basalt standard			0.12	0.02	0.18	0.05	6
BCR-2	Basalt standard			0.08	0.03	0.11	0.05	8

(‰) relative to reference material IRMM-014, defined as $\delta^{x}Fe = [(\delta^{x}Fe/^{54}Fe)_{sample}/(\delta^{x}Fe/^{54}Fe)_{IRMM\text{-}014} - 1] * 1000$ (‰), where x is either 57 or 56. Each sample solution was repeatedly measured by 3–8 times (Table 1). To assess the accuracy and long-term external precision of our analyses, two reference materials BCR-2 and BHVO-2 were processed with unknown samples for each batch of column chemistry. The long-term external precisions of $\delta^{57}Fe$ are better than 0.05‰ (2SD; Xia et al., 2017). The measured BCR-2 and BHVO-2 basalt standards yield $\delta^{57}Fe$ values of 0.11 ± 0.05‰ ($n = 8$) and 0.18 ± 0.05‰ ($n = 6$), consistent with their published values ($\delta^{57}Fe = 0.12 \pm 0.02$‰ and 0.17 ± 0.02‰; Craddock and Dauphas, 2011; He et al., 2015; Sossi et al., 2015) within uncertainty, suggesting that inter-laboratory biases for Fe isotopes are negligible.

4. RESULTS

Two fresh granodiorite porphyries yield $\delta^{57}Fe$ values of 0.03 ± 0.06‰ and 0.07 ± 0.02‰ (Table 1; Fig. 4a and b), respectively.

In the Bolong section, magnetite from the porphyries shows a large range in $\delta^{57}Fe$ values (0.25 ± 0.07‰ to 0.52 ± 0.04‰; Table 1; Fig. 4a). Chalcopyrite from the porphyries (-0.60 ± 0.07‰ to -0.42 ± 0.07‰) has a lower $\delta^{57}Fe$ signature than chalcopyrite from sandstones (-0.28 ± 0.02‰ to -0.22 ± 0.02‰) and pyrite from porphyries has a lower $\delta^{57}Fe$ (0.35 ± 0.06‰ to 0.60 ± 0.03‰) than pyrite from the sandstone (0.71 ± 0.06‰).

In the Duobuza section, magnetite from the granodiorite porphyries has relatively consistent $\delta^{57}Fe$ values ranging from 0.68 ± 0.02‰ to 0.77 ± 0.08‰, higher than magnetite from the Bolong section (Fig. 4a, b; Table 1). The $\delta^{57}Fe$ signatures of chalcopyrite from the mineralized granodiorite porphyries (-0.33 ± 0.03‰ to -0.40 ± 0.08‰) and from the sandstone (-0.38 ± 0.07‰ to -0.50 ± 0.05‰) generally overlap within error but sandstone values are slightly higher. Pyrite from the porphyries (0.53 ± 0.06‰ to 0.66 ± 0.03‰) and sandstones (0.58 ± 0.08‰ to 0.71 ± 0.07‰; Table 1) show relatively consistent $\delta^{57}Fe$ values within errors (Fig. 4b).

In both sections, pyrite has heavier and/or similar Fe isotope than magnetite, and chalcopyrite shows lightest Fe isotopic values for individual samples (Fig. 4a, b; Table 1). In addition, there is not obvious relationship between depth of samples and Fe isotopic values of minerals (pyrite, magnetite, and chalcopyrite; Table 1).

5. DISCUSSION

5.1. Fe isotope fractionation in the oxidized Duolong porphyry-high sulfidation epithermal Cu-Au deposit

Fresh granodiorite porphyries from the Duolong Cu-Au deposit have relatively constant $\delta^{57}Fe$ values ranging from 0.03 ± 0.06‰ to 0.07 ± 0.02‰ (Fig. 4a, b; Table 1), consistent with I-type intermediate-felsic rocks (from 0 to 0.2‰, mean $= 0.15 \pm 0.08$‰; Foden et al., 2015; He et al., 2017). Previous mineralogical (e.g., amphibole), petrochemical, and Sr-Nd-Hf isotopic studies show that fresh and ore-bearing granodiorite porphyries were oxidized ($fO_2 =$ NNO to NNO + 2), derived from the same source and underwent similar magmatic process (Li et al., 2011, 2013, 2016b, 2018; Sun et al., 2017), suggesting that the Duolong ore-forming magmas likely had a $\delta^{57}Fe$ value of ~0‰.

5.1.1. Fe isotope fractionation in the Bolong section

Ore-forming fluids exsolved from magmas are key to the formation of porphyry Cu-Au deposits (e.g., Sillitoe, 2010; Richards, 2011). Experimental studies have indicated that Fe is primarily present as ferrous chloride in exsolved fluids at 800 °C (e.g., Simon et al., 2004; Webster, 2004) and that Fe^{2+} preferentially incorporates the light Fe isotope (e.g., Poitrasson and Freydier, 2005; Saunier et al., 2011; Dauphas et al., 2017). Therefore, exsolved fluids may have lighter Fe isotope signatures (up to ~0.3‰; Heimann et al.,

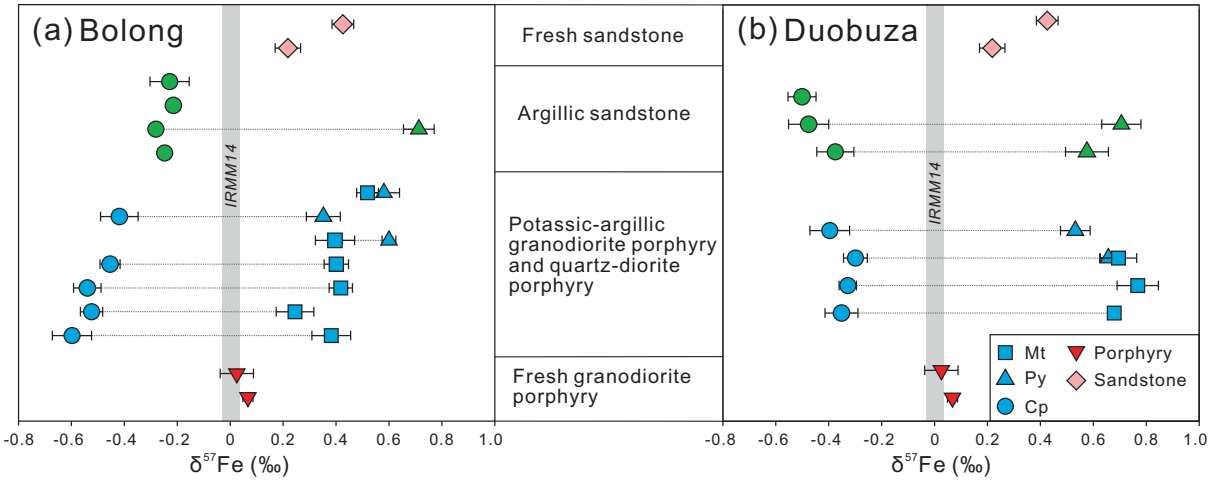

Fig. 4. Fe isotopic compositions of granodiorite porphyry, magnetite, pyrite, and chalcopyrite from the Duolong Cu-Au deposit. Dotted line indicates that the measured minerals are from the same sample. Fe isotopic data of sandstones are from Li et al. (2016a).

2008) than melts, possibly controlled by fluid salinity, the degree of exsolution, and temperature (Heimann et al., 2008; Hill et al., 2010).

There have been an increasing number of theoretical predictions on Fe isotope fractionation between mineral and fluid (Heimann et al., 2008; Syverson et al., 2013, 2017; Dauphas et al., 2017). Recent results show that Fe is almost present as the ferrous chloride in hydrothermal fluids above 300 °C (Chou and Eugster, 1977; Simon et al., 2004; Saunier et al., 2011). Therefore, fractionation factors for magnetite, pyrite, chalcopyrite, and $FeCl_4^{2-}$ in fluid (Heimann et al., 2008; Hill et al., 2010; Polyakov and Soultanov, 2011; Dauphas et al., 2017) could be adopted for evaluating Fe isotope variations in hydrothermal evolution. For a given temperature, the Fe isotope fractionation trend is pyrite > magnetite > chalcopyrite > $FeCl_4^{2-}$ in equilibrium systems (Fig. 5a, b; e.g., Polyakov and Soultanov, 2011; Dauphas et al., 2017). For the Bolong section, detailed petrography indicates that magnetite mainly occurs as disseminated and quartz–magnetite ± chalcopyrite veinlets associated with secondary biotite and K-feldspar (Fig. 3; Table 1), consistent with oxidized fluid evolution (Fig. 6a and b; Einaudi et al., 2003; Liang et al., 2009; Sun et al., 2013; Fontboté et al., 2017). Fractionation factors between magnetite and chalcopyrite in individual sample are range of 0.77–1.10‰ (Table 1), which yielded ~400–300 °C based on theoretical predictions (e.g., Dauphas et al., 2017). The calculated temperatures are significantly lower than temperatures (~550–450 °C) indicated by fluid inclusion (for magnetite-bearing samples; Li et al., 2007). Also, fractionation factors between magnetite and pyrite are −0.06 to −0.2‰ (Table 1), which give unrealistic temperatures of higher than 800 °C (e.g., Dauphas et al., 2017). Therefore, these fractionation factors likely suggest magnetite, chalcopyrite and pyrite at the Bolong section were not equilibrium precipitation, consistent with petrographic observation that is sulfide formed later than magnetite (Fig. 3d). Fe isotopic variations of these Fe-bearing minerals likely were caused by evolution of ore-forming fluids (Fig. 5).

Most magnetite from porphyries shows only weak $\delta^{57}Fe$ variation from 0.38 ± 0.07‰ to 0.52 ± 0.04‰ (Fig. 4a; Table 1), consistent with $\delta^{57}Fe$ values of ~−0.3‰ (Fig. 5a) in equilibrium fluids at ~530–480 °C. Equilibrium fluids involved in the early potassic alteration phase have lighter $\delta^{57}Fe$ values than the granodiorite porphyry ($\delta^{57}Fe = 0.03 \pm 0.06$‰ to 0.07 ± 0.02‰), supporting the hypothesis that exsolved fluids have a lighter Fe isotopic composition than the source magma (e.g., Poitrasson and Freydier, 2005; Heimann et al., 2008). As precipitation of magnetite with a heavy Fe isotopic composition (Polyakov et al., 2007; Dauphas et al., 2017) proceeds, $\delta^{57}Fe$ values of ore-forming fluids should gradually decrease (Fig. 7). One massive magnetite sample (BLZK17101-781; Fig. 3c) was selected from a porphyry with intensive quartz–magnetite ± chalcopyrite veinlets, likely suggesting it formed late in the crystallization sequence (Table 1). This magnetite has the lowest $\delta^{57}Fe$ values (0.25 ± 0.07‰), possibly indicating that it precipitated from fluids with lower $\delta^{57}Fe$ values (~−0.5‰ at ~470 °C; Fig. 5a), resulting from continuous magnetite precipitation during hydrothermal evolution (Figs. 6 and 7).

Pyrite and chalcopyrite infill inter-granular space and surround magnetite (Fig. 3d), suggesting that these minerals formed later than magnetite (Fig. 6a). Chalcopyrite from the Bolong porphyries has a relatively consistent $\delta^{57}Fe$ value of −0.60 ± 0.07‰ to −0.42 ± 0.07‰ (Fig. 4a; Table 1). The chalcopyrite with the lightest Fe isotopic composition plots close to the modelled equilibrium curve for ore-forming fluids with $\delta^{57}Fe$ values of ~−0.7‰ at

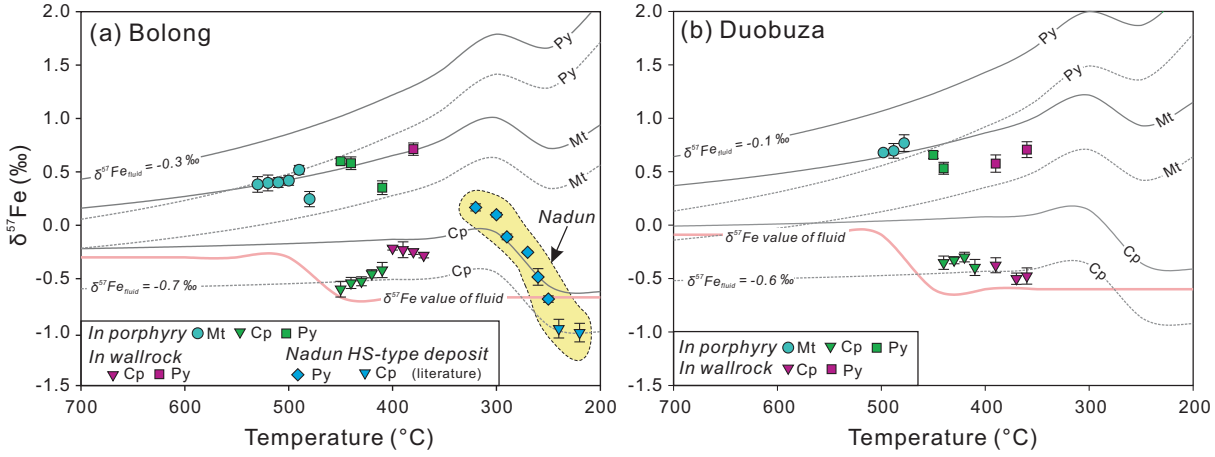

Fig. 5. $\delta^{57}Fe$ values (‰) for hydrothermal minerals vs. temperature (°C) showing Fe isotopic variations in the Duolong porphyry Cu-Au deposit (a, Bolong; b, Duobuza). Solid and dotted gray lines represent $\delta^{57}Fe$ values of minerals calculated by equilibrium fluids with various Fe isotopic compositions ($\delta^{57}Fe_{fluid} = -0.3$‰ and −0.7‰ for Bolong, −0.1‰ and −0.6‰ for Duobuza) using fractionation factors between minerals (magnetite, chalcopyrite, and pyrite) and $FeCl_4^{2-}$ in fluids (Dauphas et al., 2017). At temperature < 300 °C, $\delta^{57}Fe$ values of minerals were calculated, assuming a fluid Fe^{3+}/Fe^{2+} ratio of 0.5 (Saunier et al., 2011). Pink lines represent $\delta^{57}Fe$ values of fluids during hydrothermal evolution. Published Fe isotopic data for the Nadun high-sulfidation (HS) epithermal deposit are from Li et al. (2016a). (For interpretation of the references to colour in this figure legend, the reader is referred to the web version of this article.)

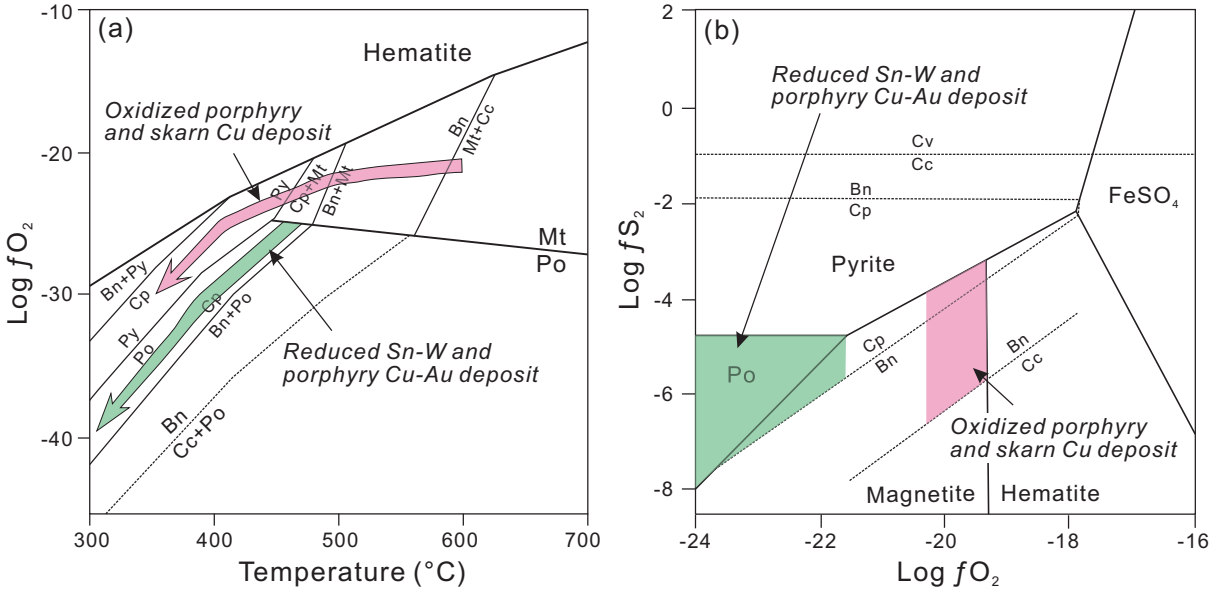

Fig. 6. (a) Temperature (°C) vs. oxygen fugacity (logfO_2) (Garwin, 2000; Wawryk and Foden, 2017) and logfO_2 vs. sulfur fugacity (logfS_2; b) (at 500 °C and 1 kb; Hemley et al., 1992) diagrams showing mineral assemblages at oxidized and reduced ore deposits.

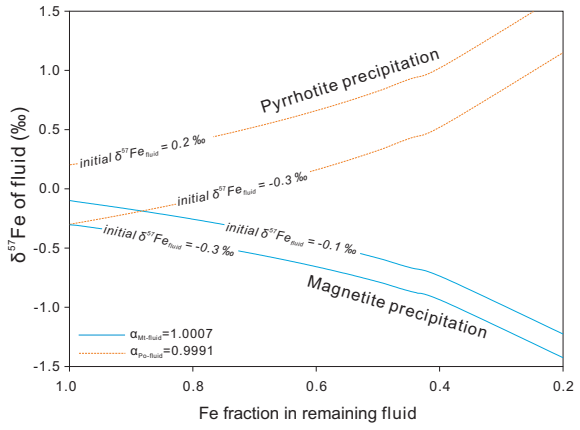

Fig. 7. Rayleigh fractionation modeling indicating that $\delta^{57}Fe$ (‰) variations in fluid caused by magnetite and pyrrhotite precipitation. The dotted pink and solid blue curves were calculated using the Rayleigh fractionation formula: $\delta^{57}Fe^{i}_{fluid} = \delta^{57}Fe^{0}_{fluid} - (1000 + \delta^{57}Fe^{0}_{fluid})$ $(1\text{-}F^{\alpha\ mineral\text{-}fluid})$, where $\delta^{57}Fe^{\ 0}_{melt}$ is the initial Fe isotopic value and F is the fraction of Fe remaining in the fluid. Fractionation factors (α) between magnetite, pyrrhotite and $FeCl^{2-}$ in fluid are from Dauphas et al. (2017) and Butler et al. (2005). (For interpretation of the references to colour in this figure legend, the reader is referred to the web version of this article.)

450–400 °C (Fig. 5a). Thus, the decreased $\delta^{57}Fe$ values (from −0.3 to −0.7‰) in ore-forming fluids are likely caused by Rayleigh fractionation of magnetite (Fig. 5a; Dauphas et al., 2017; Wawryk and Foden, 2017). The slightly different Fe isotopic composition of chalcopyrite and Fe^{2+}-bearing fluid (Fig. 5a) also suggests that chalcopyrite records the Fe isotopic value of the fluid due to a rapid isotopic exchange rate and small fractionation between them (0.09 ± 0.17‰ at 350 °C; Syverson et al., 2017). However, chalcopyrite from the mineralized wall-rock (sandstone) has a consistent $\delta^{57}Fe$ value of −0.28 ± 0.02‰ to −0.22 ± 0.02‰, higher than chalcopyrite from porphyries (Figs. 4a and 5a). Fractionation between chalcopyrite and fluid is negligible as a function of temperature (Dauphas et al., 2017; Syverson et al., 2017; Fig. 5a), thus, the higher $\delta^{57}Fe$ value in chalcopyrite from wallrock could be attributed to the interaction of ore-forming fluids with sandstone with a heavier Fe isotopic composition (~0.22 to 0.43‰; Fig. 4a; Li et al., 2016a). In addition, the Fe isotopic composition (0.58 ± 0.06‰ to 0.60 ± 0.03‰) of two porphyry pyrite samples plots on the equilibrium fractionation curve for an ore-forming fluid with a $\delta^{57}Fe$ value of ~−0.7‰ at ~440–430 °C (Fig. 5a). Previous experimental studies show that rapidly precipitated pyrite inherits the Fe isotopic composition of early formed FeS at lower temperature (~100–350 °C; Polyakov and Soultanov, 2011; Syverson et al., 2013). Owing to the sluggish pyrite-fluid isotopic exchange rate, during pyrite recrystallization, the pyrite Fe isotopic signature will only change slowly (or not at all) during reaction process (Syverson et al., 2013). At Bolong, two pyrites from the strongly argillic-altered porphyry and sandstone yielded $\delta^{57}Fe$ values of 0.35 ± 0.06‰ and 0.71 ± 0.06‰, and plot below the modelled equilibrium fractionation curve between pyrite and fluid at ~400–350 °C (Fig. 5a). Fractionation factors of ~0.77–0.99‰ between pyrite-chalcopyrite pairs in these samples (Table 1) yielded calculated temperature of ~620–530 °C, which are obviously higher than temperature (~450–350 °C) indicated by fluid inclusion (Li et al., 2007). Therefore, this may be caused by incomplete Fe isotope exchange between pyrite and ore-forming fluid at temperatures less than ~400 °C (Syverson et al., 2013).

5.1.2. Fe isotope fractionation in the Duobuza section

Similarly, fractionation factors among minerals in individual sample ($\Delta^{57}Fe_{Mt\text{-}Cpy} = 1.03$–$1.10$‰; Table 1) from the Duobuza section give the inconsistent temperatures (~300 °C) with those (~550–450 °C) indicated by fluid inclusion (Li et al., 2007). Therefore, magnetite from the porphyries has a relatively consistent $\delta^{57}Fe$ value (0.68 ± 0.02‰ to 0.77 ± 0.08‰; Fig. 4b; Table 1), similar to the $\delta^{57}Fe$ signature of equilibrium fluids at ~500–480 °C (~−0.1‰; Fig. 5b). Previous studies show that ore-forming porphyries from the Duobuza and Bolong sections were derived from the same source (Li et al., 2011, 2013, 2016b, 2018; Sun et al., 2017). Therefore, the Duobuza fluids have a slightly heavier Fe isotopic composition ($\delta^{57}Fe = \sim -0.1$‰) than fluids in the Bolong section ($\delta^{57}Fe = \sim -0.3$‰; Fig. 5a), perhaps due to a different degree of fluid exsolution (Heimann et al., 2008). Chalcopyrite from the porphyries and one sandstone sample have relatively consistent $\delta^{57}Fe$ values (-0.40 ± 0.08‰ to -0.30 ± 0.05‰; Fig. 4b; Table 1). Two chalcopyrite samples from mineralized sandstones containing low temperature quartz–chalcopyrite–pyrite–sphalerite–galena veinlets have slightly lighter $\delta^{57}Fe$ signatures (-0.50 ± 0.05‰ to -0.48 ± 0.08‰), and modeling indicates that they equilibrated with ore-forming fluids with $\delta^{57}Fe$ values of ~−0.60‰ at 440–360 °C (Fig. 5b). As described above, the lighter values likely reflect magnetite precipitation (Dauphas et al., 2017; Wawryk and Foden, 2017). In contrast, pyrite from porphyries and sandstones have $\delta^{57}Fe$ values of 0.53 ± 0.06‰ and 0.71 ± 0.07‰, close to but lower than the modeled equilibrium fractionation curve between pyrite and fluid at ~440–360 °C (Fig. 5b). Again, this disparity may reflect variations in the degree (complete and incomplete) of Fe isotope exchange between pyrite and the ore-forming fluid (Syverson et al., 2013, 2017).

5.1.3. Fe isotope fractionation in the Nadun high sulfidation epithermal Cu-Au deposit

At Nadun, a high sulfidation epithermal deposit located near to the Bolong section (Fig. 1c), pyrite and chalcopyrite associated with hematite, anhydrite, and enargite were precipitated from oxidized fluid at ~200–350 °C and chalcopyrite formed later than pyrite (Li et al., 2016a). Previous experimental studies show that ferric chloride species increase in oxidized fluids at temperatures <~300 °C and Fe^{3+} preferentially incorporates the heavy Fe isotope (Saunier et al., 2011). Therefore, mineral-fluid Fe isotope fractionation may be controlled by Fe species, temperature, and/or redox conditions (Saunier et al., 2011). Chalcopyrite from the Nadun deposit has consistent $\delta^{57}Fe$ values of -1.00 ± 0.09‰ and -0.97 ± 0.09‰ (Fig. 5a; Li et al., 2016a) and detailed fluid inclusion studies suggest that the ore-forming fluids at Nadun were produced by contraction of deep-derived vapor-rich fluids during cooling at elevated pressure above the critical curve of the salt-water system (Heinrich et al., 2004; Li et al., 2016a). The deep-derived fluids responsible for the Bolong mineralization are similar (Li et al., 2016a). Therefore, assuming $\delta^{57}Fe$ values of ~−0.7‰ and Fe^{3+}/Fe^{2+} of ~0.5 in fluids, the Nadun chalcopyrite with the lightest Fe isotopic composition equilibrated with ore-forming fluids at 250–230 °C (Fig. 5a). Meanwhile, the wide range of pyrite Fe isotope compositions ($\delta^{57}Fe = -0.69 \pm 0.03$‰ and 0.17 ± 0.03‰; Fig. 5a; Li et al., 2016a) likely resulted from more incomplete Fe isotope exchange between pyrite and ore-forming fluids at temperature <~300 °C (Syverson et al., 2013). This is corroborated by the pyrite Fe isotopic composition from many low-temperature hydrothermal systems (e.g., Butler et al., 2005; Markl et al., 2006; Rouxel et al., 2008; Polyakov and Soultanov, 2011; Syverson et al., 2017).

5.2. Fe isotopic composition as a tracer for magmatic-hydrothermal evolution

5.2.1. Comparison with Fe isotopic composition in oxidized skarn Cu-Fe and porphyry Cu-Au deposits

The Batu Hijau porphyry Cu-Au deposit (Indonesia) has similar mineral assemblages (Fig. 6a and b) as the Duolong deposit and is related to oxidized tonalite porphyry (Garwin, 2000; Wawryk and Foden, 2017). Magnetite from this deposit has a heavier $\delta^{57}Fe$ signature (from 0.24 ± 0.14‰ to 0.74 ± 0.14‰) relative to chalcopyrite (-0.62 ± 0.04‰ to -0.16 ± 0.05‰), as noted in the Duolong deposit (Fig. 4a and b). The Fe isotopic compositions are consistent with $\delta^{57}Fe$ signatures of −0.5‰ to −0.1‰ in fluids (Fig. 8), which have lighter Fe isotope than ($\delta^{57}Fe = 0.17 \pm 0.05$‰ to 0.32 ± 0.08‰) the ore-bearing intrusion (Wawryk and Foden, 2017). Moreover, the wide variation of $\delta^{57}Fe$ in magnetite and chalcopyrite were attributed to Rayleigh fractionation of magnetite during hydrothermal evolution (Fig. 7; Wawryk and Foden, 2017).

The Xinqiao skarn Cu-Fe deposit (Tongling district, China) is genetically linked to a Cretaceous monzodiorite and has oxidized mineral assemblages containing magnetite, chalcopyrite, and pyrite (Fig. 6a and b; Wang et al., 2011). Magnetite and chalcopyrite in this deposit have $\delta^{57}Fe$ values of −0.54 to 0.20‰ (±0.05‰)) and −0.98 to −0.06‰ (±0.05‰), respectively, consistent with $\delta^{57}Fe$ values of −1.20 to −0.40‰ in ore-forming fluids (Fig. 8a and b). The Fe isotopic composition of ore-forming fluids is lighter than that of the ore-bearing monzodiorite ($\delta^{57}Fe = \sim 0.15$ to 0.29‰; Wang et al., 2011), supporting the hypothesis that exsolved fluids should have lighter isotopic values than source magmas. Assuming an initial $\delta^{57}Fe$ value of −0.2‰ in the fluids, a wide range of Fe isotopic compositions in minerals might be interpreted as Rayleigh fractionation of magnetite (Figs. 7 and 8). In addition, the Fenghuangshan skarn Cu-Fe-Au deposit, located in same district, has similar mineral assemblages and similar magnetite and chalcopyrite Fe isotope compositions ($\delta^{57}Fe = -0.09$ to 0.03‰ and −1.18 to −0.05‰, respectively) as the Xinqiao deposit (Wang et al., 2015), likely suggesting that Fe isotope variation in two deposit are caused by same mechanism.

5.2.2. Comparison with Fe isotopic composition in reduced Sn-W and porphyry-skarn Cu-Au deposits

The Renison Sn-W deposit has a reduced mineral assemblage of pyrrhotite, chalcopyrite, pyrite, and minor magnetite (Fig. 6a and b; Wawryk and Foden, 2015). This

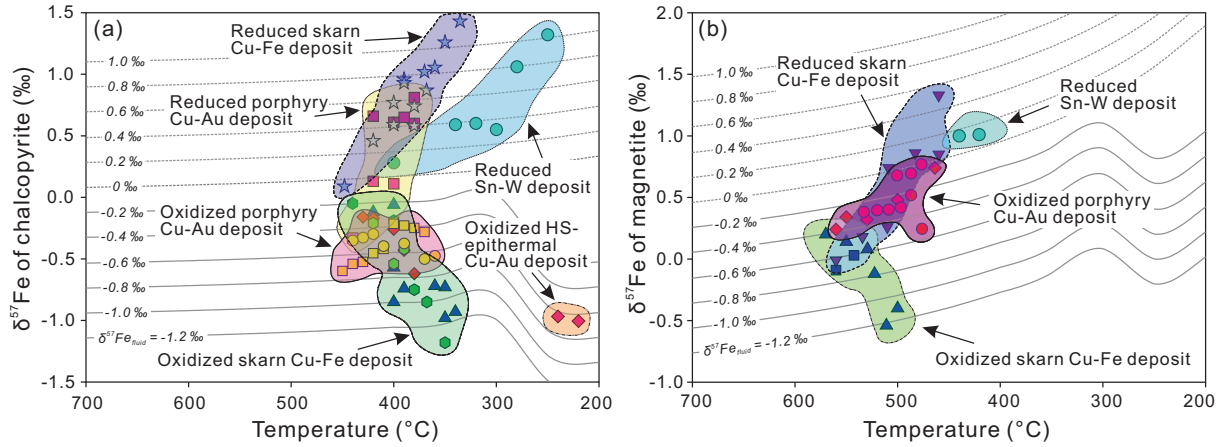

Fig. 8. δ^{57}Fe values (‰) of chalcopyrite (a) and magnetite (b) as a function of temperature (°C), showing Fe isotope variations in oxidized and reduced hydrothermal systems. Gray lines are calculated δ^{57}Fe values of chalcopyrite and magnetite by equilibrium fluids with various Fe isotopic compositions (δ^{57}Fe values ranging from −1.2‰ to 1.0‰), using fractionation factors between minerals (magnetite and chalcopyrite) and $FeCl_4^{2-}$ in fluids (Dauphas et al., 2017). In oxidized fluids with temperature < 300 °C, δ^{57}Fe values of chalcopyrite and magnetite were calculated, assuming a fluid Fe^{3+}/Fe^{2+} ratio of 0.5 (Saunier et al., 2011). Published Fe isotopic data for the oxidized (Nadun) high-sulfidation (HS) epithermal deposit, oxidized (Batu Hijau) porphyry Cu-Au deposit, oxidized (Xinqiao and Fenghuangshan) and reduced (Dongguanshan) skarn Cu-Fe deposits, reduced (Baogutu) porphyry Cu-Au deposit, and reduced (Renison) Sn-W deposit are from Li et al. (2016a), Wawryk and Foden (2017), Wang et al. (2011, 2015), Zhu (2016), and Wawryk and Foden (2015), respectively.

deposit is closely related to reduced granitic intrusions with heavier Fe isotopic values (0.27–0.45‰; Wawryk and Foden, 2015). Two magnetite samples in this deposit have δ^{57}Fe values of ~1.00‰ (±0.07‰), equilibrated with ore-forming fluids with a δ^{57}Fe value of ~0.20‰ at ~450 °C (Fig. 8b). Chalcopyrite has a wider range of δ^{57}Fe values (0.28 to 1.32‰ (±0.08‰)), consistent with ore-forming fluids with δ^{57}Fe of 0.1 to 1.00‰ at ~400–250 °C (Fig. 8a). However, pyrrhotite has the lightest δ^{57}Fe values (−1.00 to −0.15‰ (±0.08‰; Wawryk and Foden, 2015). Assuming an initial δ^{57}Fe value of ~0.2‰ in the fluids, the wide range of Fe isotopic compositions in chalcopyrite might be interpreted as Rayleigh fractionation of pyrrhotite during fluid evolution (Figs. 6a,b and 7).

The Baogutu is a rare reduced porphyry Cu-Au deposit closely associated with a diorite-granodiorite complex. The intrusion is oxidized (fO_2 = NNO + 0.5) based on amphibole and biotite compositions (Shen et al., 2015; Cao et al., 2017). One chalcopyrite from this deposit has negative δ^{57}Fe value of −0.33‰ in early potassic alteration zone with early-stage magnetite occurrence (oxidized fluids; Fig. 8a), consistent with ore-forming fluids with δ^{57}Fe = −0.4‰ (Fig. 8a). However, the occurrence of large amounts of late-stage pyrrhotite suggests that ore-forming fluids are relatively reduced, consistent with abundant CH_4-rich fluid inclusions in mineralized veins (Cao et al., 2017). Chalcopyrite has a wider range of δ^{57}Fe values (0.11 to 0.81‰ (± 0.07‰)), consistent with ore-forming fluids with δ^{57}Fe = 0 to 0.6‰ (Fig. 8a). Assuming an initial δ^{57}Fe value of −0.40‰ in the fluids, and similar to the Renison Sn-W deposit above, a wide range of Fe isotopic compositions in chalcopyrite also might be interpreted as Rayleigh fractionation of pyrrhotite (Fig. 7). Similarly, the Dongguanshan porphyry-skarn Cu-Au deposit has reduced mineral assemblages (e.g., pyrrhotite; Wang et al., 2015). Magnetite and chalcopyrite show a large δ^{57}Fe variation from −0.01 to 1.33‰ and 0.09 to 1.43‰, respectively, likely indicating that the fluids had δ^{57}Fe values from ~−0.6 to 1.0‰ (Fig. 8a and b). Again, the Fe isotopic composition of ore-forming fluids could reflect pyrrhotite fractionation if the pyrrhotite had lighter δ^{57}Fe values (~−1.39 to 0.29‰; Wang et al., 2015).

5.2.3. Fe isotopic composition as a tracer for magmatic-hydrothermal evolution

As described above, the Fe isotope composition of exsolved fluids is likely controlled by temperature, fractionation between fluid and melt, the degree of fluid exsolution, the Fe isotopic composition of the melt, and redox conditions (e.g., Heimann et al., 2008; Dauphas et al., 2017). Usually, porphyry Cu-Au deposit and skarn Cu-Fe-Au deposit are genetically linked to I-type intermediate-felsic intrusions (δ^{57}Fe values of ~0–0.2‰; Foden et al., 2015) and associated oxidized/reduced fluid systems (e.g., Li et al., 2013; Wang et al., 2011, 2015; Shen et al., 2015; Cao et al., 2017). Assuming that fractionation between the fluid and melt induces a δ^{57}Fe shift of ~0.3‰ (Heimann et al., 2008), the fluids exsolved from magmas should have δ^{57}Fe values of ~−0.3 to −0.1‰ (Fig. 9). Moreover, in oxidized systems, the δ^{57}Fe of ore-forming fluids decreases with continued magnetite crystallization during hydrothermal evolution (Fig. 7; e.g., Polyakov et al., 2007; Heimann et al., 2008; Dauphas et al., 2017). Chalcopyrite precipitated from such evolved fluids will have lighter δ^{57}Fe values (Fig. 9). In addition, for high sulfidation epithermal Cu-Au deposits, ferrous and ferric chloride species coexist in oxidized ore-forming fluids at <~300 °C (Saunier et al., 2011) and Fe isotope fractionate between ferrous and ferric chloride species (Figs. 5a, 8a, and 9) with lighter isotope preferentially entering the ferrous species. Chalcopyrite precipitated in these systems should, therefore, have a lighter Fe isotopic composition. It follows that mineral-fluid Fe isotope fractionation is likely

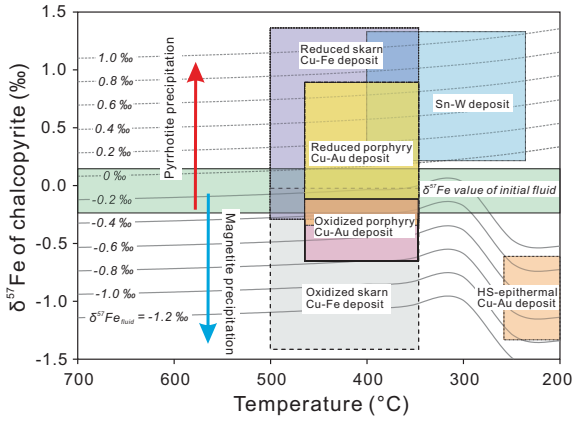

Fig. 9. δ^{57}Fe values (‰) of chalcopyrite vs. temperature (°C) diagram showing Fe isotope variation of chalcopyrite in different types of hydrothermal ore deposits. Red and blue arrows represent δ^{57}Fe variations of chalcopyrite caused by pyrrhotite and magnetite precipitation in the reduced and oxidized hydrothermal systems, respectively. (For interpretation of the references to colour in this figure legend, the reader is referred to the web version of this article.)

controlled by Fe species, temperature, and redox conditions (Polyakov et al., 2007; Saunier et al., 2011; Wawryk and Foden, 2017; Dauphas et al., 2017). However, in reduced systems (e.g., Baogutu), as ore-forming fluids evolve, δ^{57}Fe values increase due to pyrrhotite crystallization (Fig. 7; Polyakov et al., 2007; Wawryk and Foden, 2015; 2017; Dauphas et al., 2017). Thus, later precipitated chalcopyrite in a reduced system would have gradually heavier Fe isotopic as hydrothermal evolution progressed (Figs. 8a and 9).

Additionally, the reduced granites associated with Sn-W deposits generally have higher δ^{57}Fe values of ~0.3–0.5‰ than I-type intermediate-felsic intrusions (Foden et al., 2015; Wawryk and Foden, 2015; Wu et al., 2017). Therefore, the ore-forming fluids would have heavier δ^{57}Fe values (~0–0.2‰) relative to fluids associated with reduced porphyry-skarn Cu ± Fe ± Au deposits (e.g., Baotugu; Fig. 8a). Similarly, pyrrhotite crystallization will lead to elevated Fe isotopic compositions in evolved fluids, which subsequently results in heavier δ^{57}Fe values in later precipitated chalcopyrite. In summary, chalcopyrite from oxidized hydrothermal systems is characterized by an obviously lighter Fe isotopic composition than chalchopyrite from reduced hydrothermal systems (Fig. 9). It seems that δ^{57}Fe value of ~−0.2‰ in chalcopyrite might be a boundary to distinguish these two hydrothermal systems (Figs. 8a and 9). Importantly, because chalcopyrite is a common mineral in hydrothermal deposits, the chalcopyrite δ^{57}Fe could be a power tool for distinguishing oxidized and reduced fluid systems.

6. CONCLUSIONS

(1) Magnetite with potassic alteration in the Duolong porphyry Cu-Au deposit shows δ^{57}Fe values ranging from 0.38 ± 0.07‰ to 0.52 ± 0.04‰ in the Bolong section and from 0.68 ± 0.02‰ to 0.77 ± 0.08‰ in the Duobuza section. This magnetite likely equilibrated with ore-forming fluids with δ^{57}Fe values of ~−0.3‰ and ~−0.1‰ at ~530–480 °C, respectively. The equilibrium fluids had lighter δ^{57}Fe signatures than the Duolong granodiorite porphyry (δ^{57}Fe = 0.03 ± 0.06‰ to 0.07 ± 0.02‰), suggesting that exsolved fluids should have a relatively lighter Fe isotopic composition than the source magma. Late-stage magnetite in the Bolong section has the lowest δ^{57}Fe value (0.25 ± 0.07‰) and likely equilibrated with fluids with δ^{57}Fe values of ~−0.5‰ at ~470 °C. Decreasing δ^{57}Fe in ore-forming fluids is likely caused by Rayleigh fractionation of magnetite with a heavier Fe isotopic composition.

(2) Chalcopyrite from the Duolong porphyries has δ^{57}Fe values from −0.60 ± 0.07‰ to −0.30 ± 0.05‰, and equilibrium fluids had lighter δ^{57}Fe values of ~−0.7‰ to ~−0.6‰ at 450–350 °C. Variable isotope exchange (complete and incomplete) between pyrite and ore-forming fluids during sulfide precipitation leaves pyrite with heavier δ^{57}Fe values of 0.35 ± 0.06‰ to 0.71 ± 0.06‰, not reflective of values in equilibrium fluids.

(3) Chalcopyrite from reduced hydrothermal deposits always has a heavier Fe isotopic composition than chalcopyrite from oxidized hydrothermal deposits, likely controlled by the initial Fe isotopic composition of the melt and degree of pyrrhotite or magnetite precipitation. Thus, the Fe isotopic composition of chalcopyrite, a common mineral in ore deposits, could be a useful tool for distinguishing between oxidized and reduced hydrothermal systems.

ACKNOWLEDGEMENTS

This article was funded by the Natural Science Foundation Project (Grant No. 41672091; 41490613), and the Ministry of Science and Technology of China (2016YFC0600303). We obtained support and help from senior geologists Hong-Qi Chen and Yu-Bin Li at the No. 5 Geological Team, Tibet Bureau of Geology and Exploration. We also obtained specific guidance and assistance from Xin-Miao Zhao and Hui-Hui Cao concerning the Fe isotope analyses at the Institute of Geology and Geophysics, Chinese Academy of Sciences.

REFERENCES

Audétat A., Günther D. and Heinrich C. A. (2000) Magmatic-hydrothermal evolution in a fractionating granite: a microchemical study of the Sn-W-F-mineralized Mole Granite (Australia). *Geochim. Cosmochim. Acta* **64**, 3373–3393.

Butler I. B., Archer C., Vance D., Oldroyd A. and Rickard D. (2005) Fe isotope fractionation on FeS formation in ambient aqueous solution. *Earth Planet. Sci. Lett.* **236**, 430–442.

Bilenker L. D., Simon A. C., Reich M., Lundstrom C. C., Gajos N., Bindeman I., Barra F. and Munizaga R. (2016) Fe–O stable isotope pairs elucidate a high-temperature origin of Chilean iron oxide-apatite deposits. *Geochim. Cosmochim. Acta* **177**, 94–104.

Cao M. J., Qin K. Z., Li G. M., Evans N. J., Hollings P., Maisch M. and Kappler A. (2017) Mineralogical evidence for crystallization conditions and petrogenesis of ilmenite-series I-type granitoids at the Baogutu reduced porphyry Cu deposit (Western Junggar, NW China): Mössbauer spectroscopy, EPM and LA-(MC)-ICPMS analyses. *Ore Geol. Rev.* **86**, 382–403.

Chou I. M. and Eugster H. P. (1977) Solubility of magnetite in supercritical chloride solutions. *Am. J. Sci.* **277**, 1296–1314.

Cooke D. R., Hollings P. and Walsh J. L. (2005) Giant porphyry deposits: characteristics, distribution, and tectonic controls. *Econ. Geol.* **100**, 801–818.

Craddock P. R. and Dauphas N. (2011) Iron isotopic compositions of geological reference materials and Chondrites. *Geostand. Geoanal. Res.* **35**, 101–123.

Dauphas N., John S. G. and Rouxel O. (2017) Iron isotope systematics. *Rev. Mineral. Geochem.* **82**, 415–510.

Duan J. L., Tang J. X., Li Y. B., Liu S. A., Wang Q., Yang C. and Wang Y. Y. (2016) Copper isotopic signature of the Tiegelongnan high-sulfidation copper deposit, Tibet: implications for its origin and mineral exploration. *Miner. Deposita* **51**, 591–602.

Einaudi M. T., Hedenquist J. W. and Inan E. E. (2003) Sulfidation state of fluids in active and extinct hydrothermal systems: Transitions from porphyry to epithermal environments. Society of Economic Geologists Special Publication, vol. 10, pp. 285–313.

Foden J., Sossi P. A. and Wawryk C. M. (2015) Fe isotopes and the contrasting petrogenesis of A-, I- and S-type granite. *Lithos* **212**, 32–44.

Fontboté L., Kouzmanov K., Chiaradia M. and Pokrovski G. S. (2017) Sulfide minerals in hydrothermal deposits. *Elements* **13**, 97–103.

Gagnevin D., Boyce A. J., Barrie C. D., Menuge J. F. and Blakeman R. J. (2012) Zn, Fe and S isotope fractionation in a large hydrothermal system. *Geochim. Cosmochim. Acta* **88**, 183–198.

Garwin S. L. (2000) *The setting, geometry and timing of intrusion-related hydrothermal systems in the vicinity of the Batu Hijau copper-gold deposit, Sumbawa, Indonesia* PhD thesis. University of Western Australia, Perth.

Geng Q. R., Zhang Z., Peng Z. M., Guan J. L., Zhu X. P. and Mao X. C. (2016) Jurassic-Cretaceous granitoids and related tectono-metallogenesis in the Zapug-Duobuza arc, western Tibet. *Ore Geol. Rev.* **77**, 163–175.

Gong Y. Z., Xia Y., Huang F. and Yu H. M. (2017) Average iron isotopic compositions of the upper continental crust: constrained by loess from the Chinese Loess Plateau. *Acta Geochim.* **36**, 125–131.

Graham S., Pearson N., Jackson S., Griffin W. and O'Reilly S. Y. (2004) Tracing Cu and Fe from source to porphyry: in situ determination of Cu and Fe isotope ratios in sulfides from the Grasberg Cu–Au deposit. *Chem. Geol.* **207**, 147–169.

Günther T., Klemd R., Zhang X., Horn I. and Weyer S. (2017) In-situ trace element and Fe-isotope studies on magnetite of the volcanic-hosted Zhibo and Chagangnuoer iron ore deposits in the Western Tianshan, NW China. *Chem. Geol.* **453**, 111–127.

Gustafson L. B. and Hunt J. P. (1975) The Porphyry copper deposit at El Salvador, Chile. *Econ. Geol.* **70**, 857–912.

Gustafson L. B. and Quiroga J. (1995) Patterns of mineralization and alteration below the porphyry copper orebody at El Salvador, Chile. *Econ. Geol.* **90**, 2–16.

Guynn J. H., Kapp P., Pullen A., Heizier M., Gehrels G. and Ding L. (2006) Tibetan basement rocks near Amdo reveal "missing" Mesozoic tectonism along the Bangong suture, central Tibet. *Geology* **34**, 505–508.

Hao L. L., Wang Q., Wyman D. A., Ou Q., Dan W., Jiang Z. Q., Wu F. Y., Yang J. H., Long X. P. and Li J. (2016) Underplating of basaltic magmas and crustal growth in a continental arc: evidence from Late Mesozoic intermediate–felsic intrusive rocks in southern Qiangtang, central Tibet. *Lithos* **245**, 223–242.

Hedenquist J. W., Arribas A. and Reynolds T. J. (1998) Evolution of an intrusion-centered hydrothermal system: Far Southeast-Lepanto porphyry and epithermal Cu-Au deposits, Philippines. *Econ. Geol.* **93**, 373–404.

Heimann A., Beard B. L. and Johnson C. M. (2008) The role of volatile exsolution and sub-solidus fluid/rock interactions in producing high $^{56}Fe/^{54}Fe$ ratios in siliceous igneous rocks. *Geochim. Cosmochim. Acta* **72**, 4379–4396.

Hemley J. J., Cygan G. L., Fein J. B., Robinson G. R. and d'Angelo W. M. (1992) Hydrothermal ore-forming processes in the light of studies in rock-buffered systems: 1. Iron-copper-zinc-lead sulfide solubility relations. *Econ. Geol.* **87**, 1–22.

He Y. S., Ke S., Teng F. Z., Wang T. T., Wu H. J., Lu Y. H. and Li S. G. (2015) High-precision iron isotope analysis of geological reference materials by high-resolution MC-ICP-MS. *Geostand. Geoanal. Res.* **39**, 341–356.

He Y. S., Wu H. J., Ke S., Liu S. A. and Wang Q. (2017) Iron isotopic compositions of adakitic and non-adakitic granitic magmas: Magma compositional control and subtle residual garnet effect. *Geochim. Cosmochim. Acta* **203**, 89–102.

Heinrich C. A., Driesner T., Stefansson A. and Seward T. M. (2004) Magmatic vapor contraction and the transport of gold from the porphyry environment to epithermal ore deposits. *Geology* **32**, 761–764.

Hill P. S., Schauble E. A. and Young E. D. (2010) Effects of changing solution chemistry on Fe^{3+}/Fe^{2+} isotope fractionation in aqueous Fe–Cl solutions. *Geochim. Cosmochim. Acta* **74**, 6669–6689.

Hou Z. Q. and Zhang H. R. (2015) Geodynamics and metallogeny of the eastern Tethyan metallogenic domain. *Ore Geol. Rev.* **70**, 346–384.

Hou Z. Q., Gao Y. F., Qu X. M., Rui Z. Y. and Mo X. X. (2004) Origin of adakitic intrusives generated during mid-Miocene east-west extension in southern Tibet. *Earth Planet. Sci. Lett.* **220**, 139–155.

Huang F., Zhang Z. F., Lundstrom C. C. and Zhi X. C. (2011) Iron and magnesium isotopic compositions of peridotite xenoliths from Eastern China. *Geochim. Cosmochim. Acta* **75**, 3318–3334.

Huang Q. T., Cai Z. R., Xia B., Li J. F., Xia L. Z. and Liu H. C. (2015) Geochronology, geochemistry, and Sr–Nd–Pb isotopes of Cretaceous granitoids from western Tibet: petrogenesis and tectonic implications for the evolution of the Bangong Meso-Tethys. *Int. Geol. Rev.* **58**, 95–111.

Kapp P., Yin A., Harrison T. M. and Ding L. (2005) Cretaceous-Tertiary shortening, basin development, and volcanism in central Tibet. *Geol. Soc. Am. Bull.* **117**, 865–878.

Li G. M., Li J. X., Qin K. Z., Duo J., Zhang T. P., Xiao B. and Zhao J. X. (2012a) Geology and hydrothermal alteration of the Duobuza Gold-Rich Porphyry Copper District in the Bangongco Metallogenetic Belt, Northwestern Tibet. *Resour. Geol.* **62**, 99–118.

Li G. M., Li J. X., Qin K. Z., Zhang T. P. and Xiao B. (2007) High temperature, salinity and strong oxidation ore-forming fluid at Duobuza gold-rich porphyry copper deposit in the Bangonghu tectonic belt, Tibet: Evidence from fluid inclusions. *Acta Petrol Sin* **23**, 935–952 (in Chinese with English abstract).

Li G. M., Zhang X. N., Qin K. Z., Sun X. G., Zhao J. X., Yin X. B., Li J. X. and Yuan H. S. (2015) The telescoped porphyry-high sulfidation epithermal Cu(-Au) mineralization of Rongna deposit in Duolong ore cluster at the southern margin of

Qiangtang Terrane, Central Tibet: Integrated evidence from geology, hydrothermal alteration and sulfide assemblages. *Acta Petrol Sin* **31**, 2307–2324 (in Chinese with English abstract).

Li J. X. (2008) Geochronology, petrology and metallogeneses of high oxidized magma-hydrothermal fluid of Duobuza gold-Rich porphyry copper deposit in Bangonghu belt, Northern Tibet. Ph.D. thesis, Institute of Geology and Geophysics, Chinese Academy of Sciences, p. 225 (in Chinese with English abstract).

Li J. X., Li G. M., Qin K. Z., Xiao B., Chen L. and Zhao J. X. (2012b) Mineralogy and mineral chemistry of the Cretaceous Duolong Gold-Rich Porphyry Copper Deposit in the Bangongco Arc, Northern Tibet. *Resour. Geol.* **62**, 19–41.

Li J. X., Qin K. Z., Li G. M., Evans N. J., Zhao J. X., Cao M. J. and Huang F. (2016a) The Nadun Cu–Au mineralization, central Tibet: root of a high sulfidation epithermal deposit. *Ore Geol. Rev.* **78**, 371–387.

Li J. X., Qin K. Z., Li G. M., Richards J. P., Zhao J. X. and Cao M. J. (2014a) Geochronology, geochemistry, and zircon Hf isotopic compositions of Mesozoic intermediate-felsic intrusions in central Tibet: Petrogenetic and tectonic implications. *Lithos* **198**, 77–91.

Li J. X., Qin K. Z., Li G. M., Xiao B., Zhao J. X. and Chen L. (2016b) Petrogenesis of Cretaceous igneous rocks from the Duolong porphyry Cu-Au deposit, central Tibet: evidence from zircon U-Pb geochronology, petrochemistry and Sr-Nd-Pb-Hf isotope characteristics. *Geol. J.* **51**, 285–307.

Li J. X., Qin K. Z., Li G. M., Xiao B., Zhao J. X. and Chen L. (2011) Magmatic-hydrothermal evolution of the Cretaceous Duolong gold-rich porphyry copper deposit in the Bangongco metallogenic belt, Tibet: evidence from U-Pb and $^{40}Ar/^{39}Ar$ geochronology. *J. Asian Earth Sci.* **41**, 525–536.

Li J. X., Qin K. Z., Li G. M., Xiao B., Zhao J. X., Cao M. J. and Chen L. (2013) Petrogenesis of ore-bearing porphyries from the Duolong porphyry Cu-Au deposit, central Tibet: evidence from U-Pb geochronology, petrochemistry and Sr-Nd-Hf-O isotope characteristics. *Lithos* **160**, 216–227.

Li J. X., Qin K. Z., Li G. M., Evans N. J., Zhao J. X., Yue Y. H. and Xie J. (2018) Volatile variations in magmas related to porphyry Cu-Au deposits: insights from amphibole geochemistry, Duolong district, central Tibet. *Ore Geol. Rev.* **95**, 649–662.

Li S. M., Zhu D. C., Wang Q., Zhao Z. D., Sui Q. L., Liu S. A., Liu D. and Mo X. X. (2014b) Northward subduction of Bangong-Nujiang Tethys: insight from Late Jurassic intrusive rocks from Bangong Tso in western Tibet. *Lithos* **205**, 284–297.

Li S. M., Zhu D. C., Wang Q., Zhao Z., Zhang L. L., Liu S. A., Chang Q. S., Lu Y. H., Dai J. G. and Zheng Y. C. (2016c) Slab-derived adakites and subslab asthenosphere-derived OIB-type rocks at 156±2Ma from the north of Gerze, central Tibet: Records of the Bangong-Nujiang oceanic ridge subduction during the Late Jurassic. *Lithos* **262**, 456–469.

Li W. Q., Jackson S. E., Pearson N. J. and Graham S. (2010) Copper isotopic zonation in the Northparkes porphyry Cu-Au deposit, SE Australia. *Geochim. Cosmochim. Acta* **74**, 4078–4096.

Li X. K., Li C., Sun Z. M. and Wang M. (2017) Origin and tectonic setting of the giant Duolong Cu–Au deposit, South Qiangtang Terrane, Tibet: evidence from geochronology and geochemistry of Early Cretaceous intrusive rocks. *Ore Geol. Rev.* **80**, 61–78.

Liang H. Y., Sun W. D., Su W. C. and Zartman R. E. (2009) Porphyry copper-gold mineralization at Yulong, China, promoted by decreasing redox potential during magnetite alteration. *Econ. Geol.* **104**, 587–596.

Lin B., Tang J. X., Chen Y. C., Song Y., Hall G., Wang Q., Yang C., Fang X., Duan J. L., Yang H. H., Liu Z. B., Wang Y. Y. and Feng J. (2017) Geochronology and genesis of the Tiegelongnan porphyry Cu(Au) deposit in Tibet: evidence from U-Pb, Re-Os dating and Hf, S, and H-O isotopes. *Resour. Geol.* **67**, 1–21.

Liu D. L., Huang Q. S., Fan S. Q., Zhang L. Y., Shi R. D. and Ding L. (2014) Subduction of the Bangong-Nujiang Ocean: constraints from granites in the Bangong Co area, Tibet. *Geol. J.* **49**, 188–206.

Liu D. L., Shi R. D., Ding L., Huang Q. S., Zhang X. R., Yue Y. H. and Zhang L. Y. (2017) Zircon U-Pb age and Hf isotopic compositions of Mesozoic granitoids in southern Qiangtang, Tibet: implications for the subduction of the Bangong-Nujiang Tethyan Ocean. *Gondwana Res.* **41**, 157–172.

Markl G., von Blanckenburg F. and Wagner T. (2006) Iron isotope fractionation during hydrothermal ore deposition and alteration. *Geochim. Cosmochim. Acta* **70**, 3011–3030.

Poitrasson F. and Freydier R. (2005) Heavy iron isotope composition of granites determined by high resolution MC-ICP-MS. *Chem. Geol.* **222**, 132–147.

Polyakov V. B. and Soultanov D. M. (2011) New data on equilibrium iron isotope fractionation among sulfides: constraints on mechanisms of sulfide formation in hydrothermal and igneous systems. *Geochim. Cosmochim. Acta* **75**, 1957–1974.

Polyakov V. B., Clayton R. N., Horita J. and Mineev S. D. (2007) Equilibrium iron isotope fractionation factors of minerals: Reevaluation from the data of nuclear inelastic resonant X-ray scattering and Mössbauer spectroscopy. *Geochim. Cosmochim. Acta* **71**, 3833–3846.

Richards J. P. (2011) Magmatic to hydrothermal metal fluxes in convergent and collided margins. *Ore Geol. Rev.* **40**, 1–26.

Rouxel O., Shanksiii W., Bach W. and Edwards K. (2008) Integrated Fe- and S-isotope study of seafloor hydrothermal vents at East Pacific Rise 9–10°N. *Chem. Geol.* **252**, 214–227.

Rye R. O. (1993) The evolution of magmatic fluids in the epithermal environment: the stable isotope perspective. *Econ. Geol.* **88**, 733–753.

Saunier G., Pokrovski G. S. and Poitrasson F. (2011) First experimental determination of iron isotope fractionation between hematite and aqueous solution at hydrothermal conditions. *Geochim. Cosmochim. Acta* **75**, 6629–6654.

Shen P. and Pan H. (2015) Methane origin and oxygen-fugacity evolution of the Baogutu reduced porphyry Cu deposit in the West Junggar terrain, China. *Miner. Deposita* **50**, 967–986.

Sillitoe R. H. (2010) Porphyry copper systems. *Econ. Geol.* **105**, 3–41.

Simon A. C., Pettke T., Candela P. A., Piccoli P. M. and Heinrich C. A. (2004) Magnetite solubility and iron transport in magmatic-hydrothermal environments. *Geochim. Cosmochim. Acta* **68**, 4905–4914.

Sossi P. A., Halverson G. P., Nebel O. and Eggins S. M. (2015) Combined separation of Cu, Fe and Zn from rock matrices and improved analytical protocols for stable isotope determination. *Geostand. Geoanal. Res.* **39**, 129–149.

Sun J., Mao J. W., Beaudoin G., Duan X. Z., Yao F. J., Ouyang H., Wu Y., Li Y. B. and Meng X. Y. (2017) Geochronology and geochemistry of porphyritic intrusions in the Duolong porphyry and epithermal Cu-Au district, central Tibet: implications for the genesis and exploration of porphyry copper deposits. *Ore Geol. Rev.* **80**, 1004–1019.

Sun W. D., Liang H. Y., Ling M. X., Zhan M. Z., Ding X., Zhang H., Yang X. Y., Li Y. L., Ireland T. R., Wei Q. R. and Fan W. M. (2013) The link between reduced porphyry copper deposits and oxidized magmas. *Geochim. Cosmochim. Acta* **103**, 263–275.

Syverson D. D., Borrok D. M. and Seyfried W. E. (2013) Experimental determination of equilibrium Fe isotopic fractionation between pyrite and dissolved Fe under hydrothermal conditions. *Geochim. Cosmochim. Acta* **122**, 170–183.

Syverson D. D., Luhmann A. J., Tan C., Borrok D. M., Ding K. and Seyfried W. E. (2017) Fe isotope fractionation between chalcopyrite and dissolved Fe during hydrothermal recrystallization: an experimental study at 350 °C and 500 bars. *Geochim. Cosmochim. Acta* **200**, 87–109.

Telus M., Dauphas N., Moynier F., Tissot F. L. H., Teng F. Z., Nabelek P. I., Craddock P. R. and Groat L. A. (2012) Iron, zinc, magnesium and uranium isotopic fractionation during continental crust differentiation: the tale from migmatites, granitoids, and pegmatites. *Geochim. Cosmochim. Acta* **97**, 247–265.

Wang D., Sun X., Zheng Y. Y., Wu S., Xia S. L., Chang H. F. and Yu M. (2017) Two pulses of mineralization and genesis of the Zhaxikang Sb–Pb–Zn–Ag deposit in southern Tibet: constraints from Fe–Zn isotopes. *Ore Geol. Rev.* **84**, 347–363.

Wang Y., Zhu X. K. and Cheng Y. B. (2015) Fe isotope behaviours during sulfide-dominated skarn-type mineralisation. *J. Asian Earth Sci.* **103**, 374–392.

Wang Y., Zhu X. K., Mao J. W., Li Z. H. and Cheng Y. B. (2011) Iron isotope fractionation during skarn-type metallogeny: A case study of Xinqiao Cu-S-Fe-Au deposit in the Middle-Lower Yangtze valley. *Ore Geol. Rev.* **43**, 194–202.

Wawryk C. M. and Foden J. D. (2015) Fe-isotope fractionation in magmatic-hydrothermal mineral deposits: A case study from the Renison Sn–W deposit, Tasmania. *Geochim. Cosmochim. Acta* **150**, 285–298.

Wawryk C. M. and Foden J. D. (2017) Iron-isotope systematics from the Batu Hijau Cu-Au deposit, Sumbawa, Indonesia. *Chem. Geol.* **466**, 159–172.

Webster J. D. (2004) The exsolution of magmatic hydrosaline chloride liquids. *Chem. Geol.* **210**, 33–48.

Wu H., Xie C. M., Li C., Wang M., Fan J. J. and Xu W. L. (2016) Tectonic shortening and crustal thickening in subduction zones: Evidence from Middle-Late Jurassic magmatism in Southern Qiangtang, China. *Gondwana Res.* **39**, 1–13.

Wu H. J., He Y. S., Bao L., Zhu C. W. and Li S. G. (2017) Mineral composition control on inter-mineral iron isotopic fractionation in granitoids. *Geochim. Cosmochim. Acta* **198**, 208–217.

Xia Y., Li S. G. and Huang F. (2017) Iron and Zinc isotope fractionation during magmatism in the continental crust: Evidence from bimodal volcanic rocks from Hailar basin, NE China. *Geochim. Cosmochim. Acta* **213**, 35–46.

Yin A. and Harrison T. M. (2000) Geologic evolution of the Himalayan-Tibetan orogen. *Annu. Rev. Earth Planet. Sci.* **28**, 211–280.

Zhai Q. G., Jahn B. M., Zhang R. Y., Wang J. and Su L. (2011) Triassic Subduction of the Paleo-Tethys in northern Tibet, China: Evidence from the geochemical and isotopic characteristics of eclogites and blueschists of the Qiangtang Block. *J. Asian Earth Sci.* **42**, 1356–1370.

Zhang K. J., Zhang Y. X., Tang X. C. and Xia B. (2012) Late Mesozoic tectonic evolution and growth of the Tibetan plateau prior to the Indo-Asian collision. *Earth Sci. Rev.* **114**, 236–249.

Zhao X. M., Cao H. H., Mi X., Evans N. J., Qi Y. H., Huang F. and Zhang H. F. (2017) Combined iron and magnesium isotope geochemistry of pyroxenite xenoliths from Hannuoba, North China Craton: implications for mantle metasomatism. *Contrib. Mineral. Petr.* **172**, 40.

Zhao X. M., Zhang H. F., Zhu X. K., Zhu B. and Cao H. H. (2015) Effects of melt percolation on iron isotopic variation in peridotites from Yangyuan, North China Craton. *Chem. Geol.* **401**, 96–110.

Zhu B. (2016) *Application of Fe isotopes in tracing magmatic-hydrothermal ore deposits: case studies of Fe skarn and Cu porphyry deposits* PhD thesis. University of Chinese Academy of Sciences, Beijing.

Zhu B., Zhang H. F., Zhao X. M. and He Y. S. (2016a) Iron isotope fractionation during skarn-type alteration: Implications for metal source in the Han-Xing iron skarn deposit. *Ore Geol. Rev.* **74**, 139–150.

Zhu D. C., Li S. M., Cawood P. A., Wang Q., Zhao Z. D., Liu S. A. and Wang L. Q. (2016b) Assembly of the Lhasa and Qiangtang terranes in central Tibet by divergent double subduction. *Lithos* **245**, 7–17.

Zhu D. C., Zhao Z. D., Niu Y. L., Dilek Y., Hou Z. Q. and Mo X. X. (2013) The origin and pre-Cenozoic evolution of the Tibetan Plateau. *Gondwana Res.* **23**, 1429–1454.

Zhu X. P., Li G. M., Chen H. A., Ma D. F. and Huang H. X. (2015) Zircon U-Pb, molybdenite Re-Os and K-feldspar ^{40}-Ar/^{39}Ar dating of the Bolong porphyry Cu-Au deposit, Tibet, China. *Resour. Geol.* **65**, 122–135.

Associate editor: Weidong Sun